AIAA JOURNAL
Vol. 41, No. 3, March 2003

Structure of Flow over a Hypersonic Inlet with Side Compression Wedges

Y. P. Goonko,* A. F. Latypov,† I. I. Mazhul,‡ A. M. Kharitonov,§ and M. I. Yaroslavtsev¶
Institute of Theoretical and Applied Mechanics, 630090, Novosibirsk, Russia
and
P. Rostand**
Dassault Aviation, 92522 Saint Cloud, France

The flow over a hypersonic three-dimensional inlet with ramp and side-swept compression wedges was experimentally studied. Two identical inlet models were tested in the blowdown wind tunnel T-313 at Mach numbers $M_\infty = 4$ and 6 and in the hotshot wind tunnel IT-302M at $M_\infty = 6$ and 8. Optical visualization of the flow, near the inlet entrance and in the inlet duct, as well as oil-film visualization of the streamlines on compression surfaces were performed. Distributions of static pressure and heat fluxes on these surfaces in typical cross and longitudinal sections, and pitot-pressure distributions at the inlet duct exit, were obtained. Patterns of the supersonic flow over the compression wedges and in the inlet duct were identified. A characteristic feature of these flows, in particular, is what the compression wedges form shock waves glancing relative to the wedge surfaces. These shocks induce oblique separations of the boundary layer with intense helical vortices propagating far downstream. As a whole, a complex system of multiple shock and expansion waves and vortex structures occurs over the inlet section of external compression, so that the flowfield at the inlet-duct entrance, in the duct, and at the exit is significantly nonuniform. Tests with a natural development of the boundary layer on compression surfaces and with tripping were carried out. "Grater-type" trips were used, which demonstrated the high efficiency at high Mach numbers $M_\infty = 6$–8. The unit Reynolds numbers in wind tunnels at the same test Mach number $M_\infty \approx 6$ were different, $Re_{1\infty} \approx 20 \times 10^6$ 1/m in T-313 and $Re_{1\infty} = (2\text{–}2.5) \times 10^6$ 1/m in IT-302M, respectively, but the boundary-layer tripping ensured identical flow regimes determined by the state of the boundary layer. Experimental data obtained in wind tunnels of different operation principles are in good qualitative agreement even with taking into account some quantitative difference mainly attributed to the unit-Reynolds-number difference.

Nomenclature

A_0 = reference (frontal) area of inlet, m^2
c_q = heat-flux coefficient referred to the specific kinetic energy of the freestream flow, $c_q = q_w/(\rho_\infty V_\infty^3/2)$
M = flow Mach number
M_∞ = freestream Mach number
p = static pressure, N/m^2
$\bar{p}$ = relative pressure, $\bar{p} = p/p_\infty$
p_0 = total (stagnation) pressure, N/m^2
p_0' = total pressure measured with a pitot tube behind the normal shock wave in the flow with a local supersonic velocity, N/m^2
q_w = heat flux through the wall surface, J/m^{2}s
q_∞ = freestream dynamic pressure, $q_\infty = \rho_\infty V_\infty^2/2$, N/m^2
Re_t = Reynolds number of the boundary-layer transition
Re_1 = unit Reynolds number per meter, 1/m
t_0 = total (stagnation) temperature, K
V = flow velocity, m/s
γ = adiabatic exponent
δ = wedge angle, deg
ρ = flow density, kg/m^3
χ = wedge sweep angle, deg

Subscripts

0 = stagnation flow parameters
∞ = freestream parameters

Presented as Paper 98-1624 at the AIAA 8th International Space Planes, Hypersonic Systems, and Technology Conference, Norfolk, VA, 27–30 April 1998; received 21 June 2001; revision received 2 September 2002; accepted for publication 29 October 2002.

*Head of Research Group, Experimental Aerodynamics Laboratory.
†Head of Research Group of Mathematical Simulation of Ramjet/Scramjet Engines.
‡Senior Research Scientist, Experimental Aerodynamics Laboratory.
§Highest Research Scientist, Experimental Aerodynamics Laboratory.
¶Senior Research Scientist, Laboratory of Hypersonic Flows.
**Head of Aerodynamics Department. Member AIAA.

I. Introduction

ONE of the main problems that defines the prospects of bringing into existence hypersonic airbreathing vehicles is the development of a scramjet engine. Extensive investigations have been performed and are performed in this aspect. Nevertheless, gasdynamic phenomena arising in the flow around supersonic inlets and in flows with heat addition in the engine duct have not been adequately studied yet because of their complexity. This is particularly true for scramjets with three-dimensional inlets: the flow around them is complicated by three-dimensional shock–shock and shock–boundary-layer interactions.

The present paper contains the results of studying the flow around a hypersonic inlet with ramp and side compression wedges. The investigations were performed within the framework of a more general experimental study[1,2] of the resultant aerodynamic-propulsive characteristics of a model scramjet. The experiments were carried out in wind tunnels based at the Institute of Theoretical and Applied Mechanics (ITAM) of the Siberian Branch of the Russian Academy of Sciences. Tests in a hot-shot wind tunnel, IT-302M, at freestream Mach numbers $M_\infty = 6$ and 8 included both regimes with combustion of gaseous hydrogen and without fuel supply; tests in a blowdown wind tunnel, T-313, at $M_\infty = 4$ and 6 were conducted in regimes without fuel addition. The engine model was assembled from three modular sections, and the test program included experiments with the complete scramjet model (inlet + combustor + nozzle) and its components: engine without the nozzle (inlet + combustor) and inlet alone. Comparative tests of two identical inlet models of equal dimensions in IT-302M and T-313 at $M_\infty = 6$ were performed.

One of the objectives of the study[1,2] was to obtain experimental data for a generic complex hypersonic integrated configuration, which would include a scramjet. In Ref. 1 such a configuration was called integration validation object (IVO); it should be adequately representative to determine and confirm the capabilities of numerical methods for computation of the aerodynamic-propulsive characteristics for hypersonic airbreathing vehicles. The IVO concept is derived from the analysis of requirements to the accuracy of determination and prediction of the characteristics as applied to hypersonic airbreathing vehicles.[3,4] Difficulties arising thereby are related, in particular, to the fact that the resultant acceleration for such a vehicle is produced by a small difference in two large quantities: engine thrust and airplane drag. Ground-based testing of the IVO model should incorporate the problems inherent in hypersonic airbreathing vehicles: flow physics, thermogasdynamics, interaction of various elements of the engine, formation of aerodynamic drag and propulsion thrust forces, etc. At the same time the IVO configuration should be rather simple and convenient for computations to be compared with controllable experimental data. A model scramjet including a three-dimensional inlet with side compression wedges, which was similar to inlets of Ref. 5–9, was developed as an IVO to be tested in ITAM wind tunnels.

The model parameters were chosen in such a way that both the inlet and the engine itself were workable under test conditions, but the objective of reaching a higher efficiency as compared to other types of inlets was not pursued therewith. The study of the model scramjet in wind tunnels of different operation imposed the requirement that reasonable performance of the model within the Mach-number range examined was ensured with a fixed geometry of the inlet. Therefore, the necessary compression of the airstream captured by the inlet and, hence, relative cross-sectional areas of the inlet duct at the entrance and in the throat were chosen as applied to both test conditions: testing the model engine with combustion in IT-302M and providing the inlet starting at the lowest Mach numbers of the examined range, that is, at $M_\infty = 4$ in T-313.

II. Models and Test Conditions

The inlet models tested have an identical configuration, size, and construction; they were mounted in an identical manner on pylons struts, but the latter were different in accordance with different model-support arrangements in IT-302M and T-313. A general view of the model configuration is shown in Fig. 1, a drawing with main dimensions is displayed in Fig. 2, and basic geometrical parameters of the inlet are also tabulated in Table 1.

The inlet has a ramp wedge and side wedges of initial external compression. An internal duct of the inlet covered by a cowl begins from the entrance cross section "E-E" marked in Fig. 2 and arranged at a distance $L_{cl} = 255.8$ mm from the leading edge of the ramp wedge. The cowl lip is bent by an angle $\delta_{cl} = 9$ deg chosen under the condition of model inlet starting in T-313 at the smallest Mach number examined, $M_\infty = 4$. Behind the inlet throat there is a diffuser with a small inclination of the lower wall at an angle $\delta_{dif} = 2$ deg. Cross sections of the duct in the throat and in the diffuser are rectangular. Note, the relative exit area of the inlet diffuser $\bar{A}_{ex} = 0.123$ as compared to the relative throat area $\bar{A}_{th} = 0.10$ was chosen by taking into account the total degree of area expansion for the engine channel of the complete scramjet model presented in Ref. 1. A combustion chamber of the engine begins from a stepwise expansion immediately behind the exit cross section of the inlet duct. The total area expansion should be sufficient in order to prevent, for the cases of testing the complete model with combustion in IT-302M, the influence of thermal choking of the combustion chamber on the external flow around the inlet.

The configuration of the model inlet resembles that of inlet Ref. 5, which was designed for a Mach number $M_\infty = 5$ and also had a ramp and side compression wedges. The presence of the ramp wedge of external compression and some internal compression in these inlets give them properties similar to two-dimensional (flat) inlets with mixed external and internal compression. The inlets of Refs. 6–9, in contrast to the inlet under consideration, have no ramp wedge, and they are inlets of primarily internal compression.

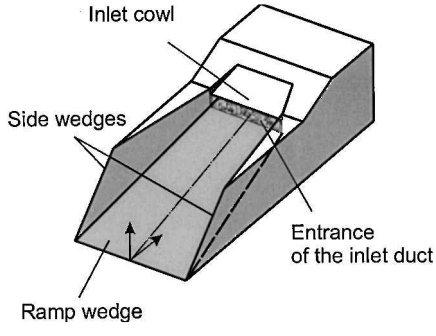

Fig. 1 General view of the model inlet.

Table 1 Basic geometrical parameters of the inlet

Definition of parameter	Value
Ramp wedge angle δ_{rw}, sweep angle χ_{rw}	$\delta_{rw} = 12.5$ deg, $\chi_{rw} = 0$
Angles of side wedges δ_{sw}, χ_{sw}	$\delta_{sw} = 10$ deg, $\chi_{sw} = 45$ deg
Reference dimensions of the inlet determined by leading edges of compression wedges:	
Width of the ramp wedge b_{inl}	153.8 mm
Height of the side wedges h_{inl}	80 mm
Reference area $A_0 = b_{inl} h_{inl}$	0.012304 m^2
Relative cross-sectional area of the inlet-duct entrance $\bar{A}_{en} = A_{en}/A_0$	0.184
Relative throat area $\bar{A}_{th} = A_{th}/A_0$	0.1
Relative duct exit area $\bar{A}_{ex} = A_{ex}/A_0$	0.123

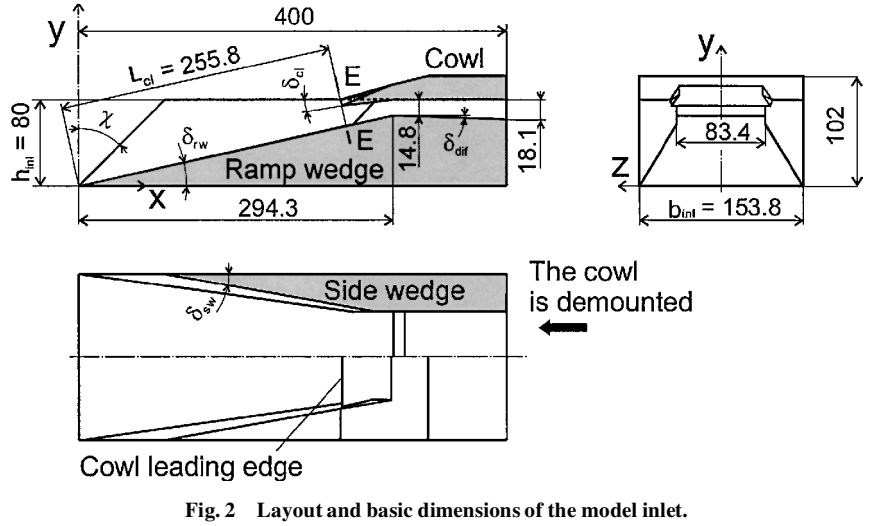

Fig. 2 Layout and basic dimensions of the model inlet.

Table 2 Test conditions

Wind tunnel	Mach number M_∞	Total pressure $p_{0\infty}$, N/m^2	Total temperature $t_{0\infty}$, K	Unit Reynolds number $Re_{1\infty}$, 1/m
T-313	4.04	10.6×10^5	280–295	$(4.7–5.4) \times 10^7$
	5.89	8.3×10^5	280–295	$(1.8–2) \times 10^7$
IT-303M	5.6–5.8	$(19.8–68.0) \times 10^5$	1300–1730	$(1.9–2.5) \times 10^6$
	7.71–7.89	$(54.0–117.6) \times 10^5$	2270–2320	$(1.2–1.4) \times 10^6$

One of the inlet models was tested in the blowdown wind tunnel T-313 (Ref. 10) with test-section dimensions $0.6 \times 0.6 \times 2.5$ m. The main flow parameters in these tests are listed in Table 2. The quality of flowfield in the test section of T-313 can be characterized by deviations of the Mach number, which do not exceed 0.5% for $M_\infty = 4$ and 1% for $M_\infty = 6$.

The static-pressure distribution over the compression wedges of the inlet and in the internal duct and also the pitot-pressure distribution at the inlet-duct exit were measured for the inlet model tested in T-313. A pressure meter MID-100, which ranks among permanent equipment of the facility and is described in Ref. 11, was used. Static-pressure taps 1 mm in diameter were positioned in two longitudinal sections: in the plane of symmetry and in a section shifted by 20 mm from the plane of symmetry; in a cross section at a distance $x = 105$ mm from the ramp leading edge; and in a set of cross sections in the inlet duct. The maximum total rms error of measuring the relative static pressure $\bar{p}$, including the random and instrumental components and the error caused by flowfield nonuniformity in the wind tunnel, is estimated as $\sigma(\bar{p}) = 0.15$ based on the data[12] for $M_\infty = 4$ and does not exceed $\sigma(\bar{p}) = 0.6$ for $M_\infty = 6$. In correlation with the level of $\bar{p}$ obtained for $M_\infty = 4$ and 6, these errors are less than 5 and 12% in pressure measurement on the compression ramp and side wedges and less than 1 and 2% in pressure measurement in the inlet duct. The maximum total rms error in pitot-pressure measurement is less than $\sigma(p_0'/p_\infty) = 0.003$.

Because of the construction of the inlet, it was not possible to observe the flow between the side compression wedges through a schlieren device. A limited region of flow outside the optical shadow of the model, above the side compression wedges in the vicinity of the entrance cross section, could be observed. Therewith, as for shock waves forming between the side compression wedges, only continuations of some of them coming beyond the model shadow were seen. The inlet model tested in T-313 was equipped by optical glasses in the side walls, which allowed us to observe the flow in the throat and in the diffuser of the inlet duct in this case. Oil-film visualization of the surface streamlines on compression wedges, near the entrance, and in the inlet duct was also performed.

The other inlet model was tested in the hotshot wind tunnel IT-302M (Ref. 13). The tests in this wind tunnel were performed at $M_\infty = 6$ and 8 in regimes with pressure stabilization in the plenum chamber of the wind tunnel; the test regime of the flow around the model was stabilized 20–50 ms after wind-tunnel starting and lasted up to 100–135 ms. The tests at $M_\infty = 6$ were conducted using a contoured nozzle with a 300-mm exit diameter, and a conical nozzle with a 330-mm diameter was used for $M_\infty = 8$. The flow parameters in two test series were ranged as presented in Table 2.

The deviations of local freestream Mach numbers from the mean values over the flow core at the nozzle exit in IT-302M are from -0.9 to $+1.5$% for $M_\infty = 6$ and from -1.5 to $+1.7$% for $M_\infty = 8$; the errors of determining the dynamic pressure q_∞ do not exceed 7.3 and 2.6%, respectively.

The inlet model tested in IT-302M was equipped by small-scale fast-response pressure gauges mounted in special containers inside the model. Ten pressure taps were located in the plane of symmetry: on the ramp, on the lower surface of the inlet duct, and on the internal surface of the cowl. The pressure gauges used are described in Ref. 14; their total error of pressure measurement is about 5% of a nominal value. Heat-flux measurements were also performed at testing the model in IT-302M using calorimetric gauges of a type as in Ref. 15; their characteristics were studied in Ref. 16. These gauges, 4.5 mm in diameter, were located in the longitudinal section shifted by 20 mm from the plane of symmetry (eight metering points on the ramp and lower surface of the inlet duct and three points on the internal surface of the inlet cowl). The possible error in wall-temperature measurement was less than 3%, and the error of heat-flux reconstruction was about 10%. The special features of determining freestream parameters in IT-302M and heat fluxes in hotshot tunnels are discussed in Ref. 17.

Schlieren visualization of the flow in the vicinity of the entrance cross section above the side compression wedges and oil visualization of the limiting streamlines on compression-wedge surfaces were also carried out in IT-302M. The latter was performed with lampblack-oil spots 5–7 mm in diameter, which spread along surface streamlines in the course of testing.

The test conditions at Mach numbers $M_\infty = 6$ in T-313 and at $M_\infty = 6$ and 8 in IT-302M are characterized by rather low values of the Reynolds number. Owing to this, as was shown by preliminary calculated estimates, a laminar or transitional state of the boundary layer on compression wedges of the inlet should be expected. Therefore, in the preceding regimes the inlet was tested both with and without boundary-layer tripping.

III. Some Calculated Estimates of the Inlet Flow Parameters

To facilitate interpretation of the experimentally observed pattern of the flow around the inlet, the position and interaction of shock waves formed by the ramp and side compression wedges were calculated. An example of the flow pattern calculated for $M_\infty = 6$ is shown in Fig. 3 as a) the side view of the model cut in the plane of symmetry, b) the cross-sectional profile, and c) the top view. In the latter case, one-half of the model is shown because of its symmetry. The letter symbols in Fig. 3 denote characteristic surfaces, lines, and points of the model contour and shock waves; symmetrically opposing points on the other half of the model will be designated by primed letters. These notations will be used further to discuss both calculated and experimental results.

The ramp compression wedge with an angle δ_{rw} and with a nonswept leading edge AA' forms an oblique shock wave *rws* being plane (Figs. 3a and 3b). The side compression wedges with an angle δ_{sw} and swept leading edges AB and $A'B'$ form shock waves *sws* and *sws'* being also plane but inclined in a cross section in accordance with the slope of the compression surfaces ABG and $A'B'G'$ (Figs. 3b and 3c). The latter shocks can be called spatially oriented plane shock waves, which are determined analytically exactly in the flow regions that do not experience tip effects. We used the relations[18,19] formulated in terms of vector algebra and reduced the problem of a spatially oriented plane shock wave to the problem of an oblique

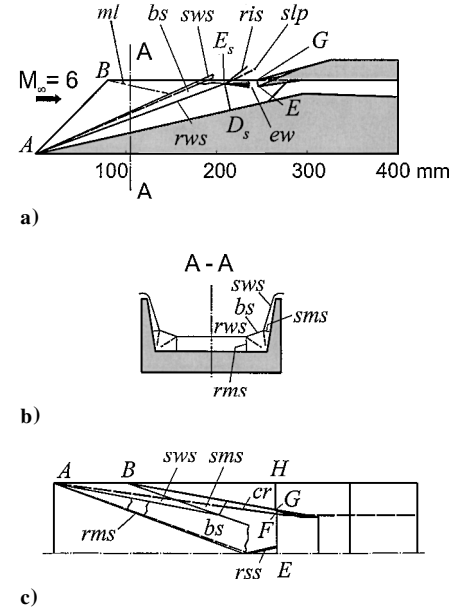

Fig. 3 Calculated shock-wave structure in the inviscid flow over the external compression wedges of the inlet, $M_\infty = 6$.

shock wave in a two-dimensional flow. The interaction of the shock waves *rws* and *sws* in the dihedral corner is irregular, of Mach-reflection type in the cross section; as a result, a bridging shock wave *bs* and reflected shock waves *rms* and *sms* form, as is shown in Fig. 3b. The shock waves *rms*, *sms*, *bs* originate at the corner vertex A (and, respectively, *rms′*, *sms′*, *bs′* at A') as conical ones, but they can be curved in the cross section. They were calculated assuming that they are also spatially oriented plane shock waves, and the flow behind them is deflected from a direction of either the flow behind the shock *rws* or the flow behind the shock *sws* to the direction of the dihedral corner rib *cr*. The shocks *rms* and *sms* are glancing with respect to plane surfaces of the compression wedges. The position of the bridging plane shock *bs* is determined by points of intersection of the shocks *rms* and *sms* with the shocks *rws* and *sws*, respectively. The flow behind the plane shock *rws* in the region between the ramp leading edge and the crossing shocks *rms* and *rms′*, up to the line E_sD_s of intersection of the latter in the plane of symmetry, is uniform, and its parameters are calculated analytically exactly.

In the region of intersection of the crossing shocks *rms* and *rms′* at the plane of symmetry, the flow pattern becomes much more complicated. The point E_s of intersection of the shocks *rws*, *rms*, *bs* and, respectively, *rms′*, *sms′*, *bs′*, which is shown in Fig. 3a, is singular and can be called the point of multiple interaction of flows and shock waves. First, in the flow under the point E_s the shocks *rms* and *rms′* intersect and reflect at the plane of symmetry with the formation of secondary reflected side shocks *rss* and *rss′*. (The shock *rss* is shown on the top view in Fig. 3c.) Second, in the flow above the point E_s the bridging shocks *bs* and *bs′* collide with each other, and interaction of flows behind them occurs. A resultant shock wave *ris* arises here (see Fig. 3a), which has a greater inclination in the plane of symmetry and a greater intensity than the shock wave *rws*; an expansion wave *ew* and a velocity–discontinuity sheet with a slip line *slp* in the symmetry plane form also. Interaction of flows and spatially oriented shock waves upstream and downstream of the point E_s is actually three-dimensional, but it was calculated under the assumption that the flow behind the shock wave *ris* is two-dimensional. The calculated structure of this interaction at the plane of symmetry is shown in Fig. 3a. The expansion wave *ew* can partially (at $M_\infty = 6$) or completely (at $M_\infty = 4$) enter the inlet duct.

The top view in Fig. 3c shows the lines of intersection of shock waves with the plane of the ramp wedge and with the horizontal plane passing through the vertices B and B' of the side wedges. Both for $M_\infty = 4$ and 6, the shock waves *rss* and *rss′* reflected from the plane of symmetry fall on the inlet-duct entrance and cross the leading edge of the cowl lip (line FEF').

Interaction of flows and shock waves at the point E_s can be influenced by tip effects propagating from the vertices B and B' and developing along the edges BG and $B'G'$ of the side wedges. Such an effect manifests itself inside a Mach conoid emanating from a wedge vertex, and its action at a wedge surface begins from a Mach line *ml* determined in the flow behind the shock wave *sws* and drawn in Fig. 3a.

Thus, the calculations showed that initial shock waves formed by compression wedges interact with each other in a complex manner with the formation of reflected shock waves, which are glancing with respect to the wedge surfaces. As a result, multiple interacting shock waves in front of the inlet-duct entrance lead to the formation of a significantly nonuniform flowfield here.

IV. State of Boundary Layer and Its Glancing-Shock-Induced Separation

Because intensive shock waves forming in the flow over the compression wedges are glancing with respect to wedge surfaces, they might induce a three-dimensional boundary-layer separation, which can be named oblique. In this context we obtained the simplest estimates of the possible state of the boundary layer developing on compression surfaces and the characteristics of the said oblique separation.

The state of the boundary layer on the model was evaluated using the experimental results[20,21] on measurement of the boundary-layer transition in T-313. A flat plate with a sharp leading edge was tested within the Mach range $M_\infty = 2.5$–6 for $Re_{1\infty} = 1.1 \times 10^6$ and 1.6×10^7 1/m. The data for $M_\infty = 6$ obtained by of V. I. Kornilov were not published, but they were used with his permission. The transition Reynolds numbers obtained correspond to the known power dependence of the unit Reynolds number $Re_t \sim Re_1^n$ with an exponent $n \approx 0.4$; the validity of this dependence for $M_\infty = 3$ and 4 in T-313 was demonstrated in Ref. 22. We also note that the bluntness of the leading edges of the inlet model tested was rather small $h_{bl} = 0.12 \pm 0.01$ mm and, according to the data,[20] had a very subtle effect on transition.

The following estimates of the transition Reynolds numbers and lengths were obtained for a flow behind the shock wave on the ramp wedge of the model considered:

$$M_\infty = 4, \qquad M_{rws} = 3.14, \qquad Re_{1rws} = 7.0 \times 10^7 \text{ 1/m}$$

$$Re_t = (3.6\text{–}5.6) \times 10^6, \qquad L_t = 50\text{–}80 \text{ mm}$$

$$M_\infty = 6, \qquad M_{rws} = 4.26, \qquad Re_{1rws} = 2.6 \times 10^7 \text{ 1/m}$$

$$Re_t = (3.0\text{–}4.7) \times 10^6, \qquad L_t = 115\text{–}180 \text{ mm}$$

Here M_{rws} and Re_{1rws} are the Mach number and the unit Reynolds number behind the shock wave *rws*; the intervals indicated for Re_t and L_t correspond to the transition beginning and end.

The effect of swept leading edges for the side compression wedges was taken into account on the basis of the experimental data[21] for a flat plate with a variable-sweep leading edge. These data show that the ratio of the transition Reynolds numbers $(Re_t)_{\chi \neq 0}/(Re_t)_{\chi = 0}$ at a given sweep angle χ is a little different for $M_\infty = 3$ and 4, and the value $(Re_t)_{\chi = 45 \text{ deg}}/(Re_t)_{\chi = 0} \approx 0.4$ determined for an angle $\chi = 45$ deg at $M_\infty = 4$ was also used for $M_\infty = 6$. Correspondingly, the transition Reynolds numbers on the side wedges were expected to be smaller than half of those for the ramp wedge.

Thus, according to the estimates calculated for the model tested in T-313 we expected the flow over compression wedges with a laminar-turbulent boundary layer in the case of natural development of the latter. Similar estimates of the boundary-layer state as applied to test conditions in the hot-shot wind tunnel IT-302M showed that we could expect the flow with a laminar boundary layer on compression wedges beyond the entrance cross section of the inlet.

There are many papers dealing with oblique turbulent separation, and correspondingly, there are different dependences for estimating its parameters. In the present paper these estimates were obtained in accordance with the study[23] of corner flows, including glancing shock waves that interacted with the boundary layer, at Mach numbers $M_\infty = 2$–4 in the T-313 wind tunnel. The results of this study on estimating parameters of the oblique turbulent separation were tested by comparison with the data of other authors and published in Ref. 24; the use of these results under the conditions considered is justified. It is well known for supersonic corner flows that, if the region of interaction of a glancing shock wave with the boundary layer is reasonably extended and the turbulent boundary layer is developed, one can assume this flow to be close to conical. In this case the two-dimensional analogy is valid: the pressure distribution in the separation region on a flat surface in the direction perpendicular to the line of shock/surface intersection is the same as that in two-dimensional separation flows. In particular, two-dimensional relations are valid for pressure estimation in the so-called isobaric zone of separation (pressure plateau), if the reduced velocity component normal to the shock/surface intersection line is used. The plateau pressure and position of the separation lines were estimated using the simplest dependences presented in Ref. 24:

$$\bar{p}_{plt} = 0.6M_n + 0.7 \tag{1}$$

$$\gamma/\beta^* = 1 + 0.53 \cdot \left(lg\,\bar{p}_s \big/ lg\,\bar{p}_s^* - 1\right) \tag{2}$$

Here M_n is the said normal Mach number component of flow upstream of the glancing shock; $\bar{p}_{plt}$ is the relative plateau pressure; $\bar{p}_s$ is the strength of the glancing shock (ratio of the pressure downstream of the shock to the pressure upstream of it); $\bar{p}_s^*$ and β^* are the strength and the inclination angle of the critical glancing shock corresponding to the beginning of emergence of turbulent separation for a given Mach number, and the inclination angle is an angle

between the upstream flow direction and the shock in the plane relative to which it is glancing; and γ is the angle of inclination of the separation line. To estimate the critical values in Eq. (2), we, as well as the authors of Refs. 23 and 24, used the Korkedgi formula (of Ref. 25):

$$M \cdot \delta^* = 0.3 \tag{3}$$

where δ^* is the critical value of the angle of the wedge that generated a glancing shock wave responsible for oblique separation of the boundary layer. The experimental data[23,24] are in good agreement with this dependence.

For test conditions of the model in T-313 at $M_\infty = 6$, the calculated estimates of the laminar separation characteristics with the use of the two-dimensional analogy just mentioned were obtained. The experimental data[26] on three-dimensional separation with interaction between a glancing plane shock wave and a laminar boundary layer for $M_\infty = 2.25$ and $Re_\infty = (6–30) \times 10^6$ were used. In our case, for example, the Reynolds number (determined for the first measurement cross section $x = 105$ mm) corresponds to $Re = 27 \times 10^6$. In the case of laminar separation in a two-dimensional flow, the plateau pressure remains almost unchanged for Mach numbers $M_\infty < 1.4$ (e.g., see Ref. 27). For the test conditions[26] the Mach number normal to the shock was $M_{\infty n} = 1.1–1.2$, and for the inlet model tested at $M_\infty = 6$ we had $(M_{\text{rws}})_n \approx 1.3$. Therefore, in accordance with Ref. 26, we assumed that the plateau pressure of laminar separation was equal to

$$\bar{p}_{\text{pll}} = \text{const} = 1.15 \tag{4}$$

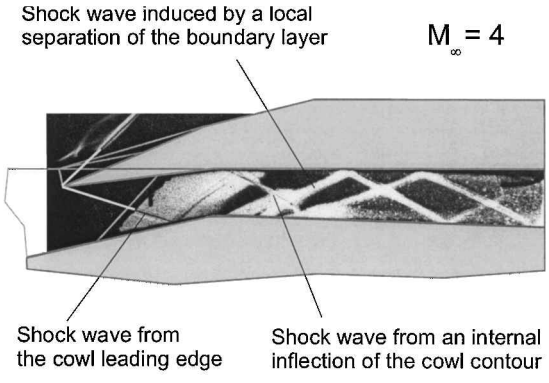

Fig. 4 Photographed flow picture in the inlet duct for $M_\infty = 4$.

V. Test Results

A. Inlet Starting

The schlieren flow visualization has shown that there is no detached bow shock wave at the inlet-duct entrance, and a supersonic flow with oblique shock waves forms in the duct. This means that the inlet has been started in both wind tunnels within the entire test range of freestream velocities. A photographed flow picture in the inlet duct for the smallest Mach number examined, $M_\infty = 4$, is presented in Fig. 4. The first internal shock wave is generated by the inlet cowl lip; another arises at the inflection edge of the upper wall of the duct. There is also a shock wave induced by a local cross separation of the boundary layer on the lower wall of the duct immediately behind the inlet throat; this separation is induced by an intensive oblique shock wave falling on the wall somewhat downstream (Fig. 4). Oil-film visualization also confirms the inlet starting. A typical oil-film picture of the limiting streamlines on surfaces of the compression wedges and lower wall of the duct also for $M_\infty = 4$ is presented in Fig. 5. It was obtained in a test of the model in T-313 without boundary-layer tripping. The position of the

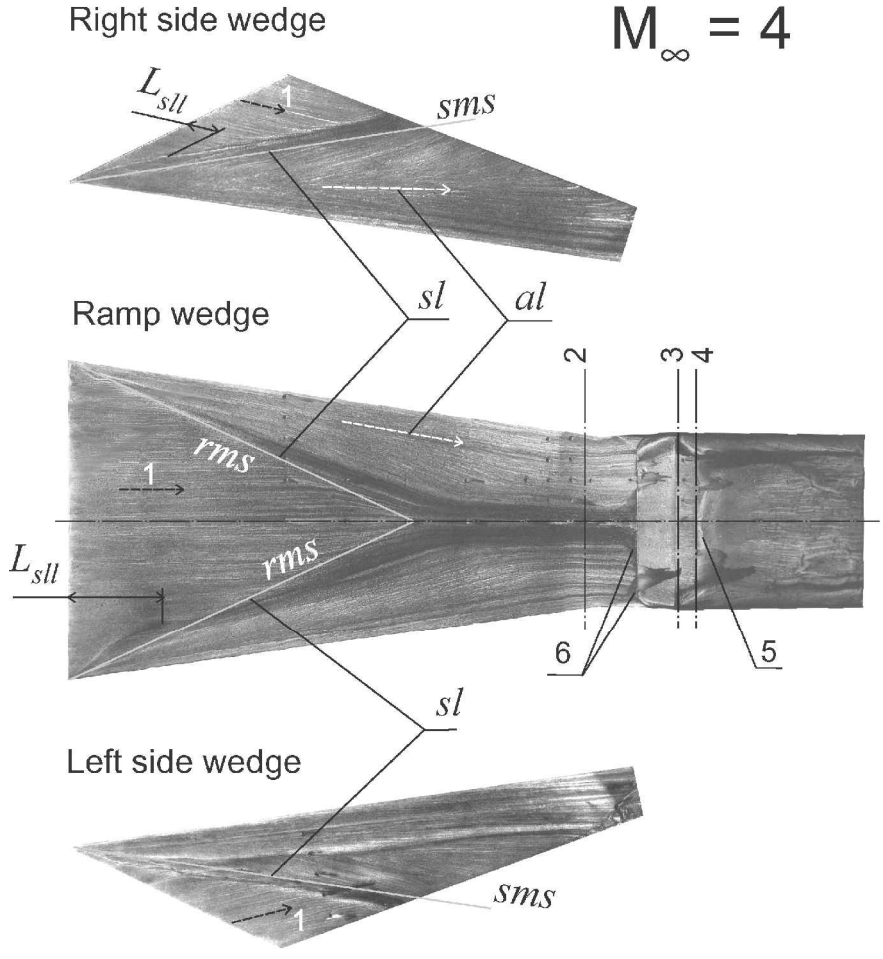

Fig. 5 Oil-film picture of limiting streamlines on surfaces of the compression wedges. $M_\infty = 4$, no boundary-layer tripping: 1, flow direction at the wedge leading edge; 2, position of the entrance cross section; 3 and 4, initial and final cross sections of the inlet throat; 5, cross separation immediately behind the inlet throat; and 6, spanwise-extended separation of the boundary layer with a waved separation line.

inlet-duct entrance is marked. The streamlines on the ramp wedge in front of the entrance are smooth, that is, at this place there is no cross separation of the boundary layer that could be induced by a normal shock wave.

B. Flow over the Compression Wedges

1. Tests Without Boundary-Layer Tripping

The oil-film picture of the surface streamlines on the compression wedges, presented in Fig. 5 for $M_\infty = 4$, corresponds to natural development of the boundary layer. The lines *sl* of oblique separations of the boundary layer, emanating from the vertices of wedge corners, are S shaped. By the data of Ref. 24, it is typical of a separation induced by a glancing shock wave at its interaction with the boundary layer initially laminar with a transition to a turbulent one. The lengths L_{sll} corresponding to the laminar portion of separation lines are marked in Fig. 5. They give a rough estimate of the laminar boundary-layer length equal to 15–45 mm as compared to the predicted value $L_t = 50$–80 mm for the ramp wedge and to 10–12 mm as compared to $L_t \approx 20$–35 mm for the side wedges. Positions of the calculated reflected shock waves *rms* and *sms* are also marked in Fig. 5. The separation lines on the ramp wedge run at first upstream and thereafter downstream of these shock-wave traces, which can be explained by the transitional boundary layer. There was no well-defined plateau in the pressure distribution across the ramp wedge in the measurement cross section $x = 105$ mm in this case, but typical inflections in the pressure curve were observed on the right and left from the plane of symmetry. The pressure level at these inflections was in good agreement with the calculated estimate $\bar{p}_{plt}$ [Eq. (1)] for a developed oblique turbulent separation.

The oblique separation lines on the ramp wedge bend near the place of intersection of the shock waves *rms* approaching asymptotically the axes of symmetry. There are attachment lines *al* after the oblique separation lines. In zones between the separation and attachment lines, typical S-shaped streamlines are seen, which demonstrate that helical vortices form here. The latter develop far downstream up to the inlet entrance.

The oil-film picture for the ramp wedge obtained at $M_\infty = 6$ in a test without boundary-layer tripping is presented in Fig. 6. In this case the separation lines *sl* emanating from the vertices of wedge corners are arc shaped, which is typical of the laminar boundary layer.[23,26] This is compatible with the preceding estimates of the boundary-layer transition length, in particular, $L_t \approx 135$–210 mm for the ramp wedge in T-313 for $M_\infty = 6$. Note that internal separation and reattachment lines cased by secondary oblique separations of the boundary layer are observed in the main oblique separation regions (Fig. 6). Arc-shaped separation lines were also obtained for $M_\infty = 6$ and 8 in IT-302M at testing the model without boundary-layer tripping.

The laminar character of oblique separation at $M_\infty = 6$ in T-313 in tests without boundary-layer tripping is also confirmed by the pressure distribution in the measurement cross section $x = 105$ mm (Fig. 7). The pressure plots are combined with the calculated cross-flow shock-wave structure (Fig. 7a). The pressure levels upstream and downstream of the shock waves *rws*, *rms*, *sws*, and *sms*, respectively $\bar{p}_{rws}$, $\bar{p}_{rms}$, $\bar{p}_{sws}$, and $\bar{p}_{sms}$, are marked in the graphs of pressure distributions across the ramp (Fig. 7b) and the side compression wedge (Fig. 7c). On the ramp wedge the measurement cross section intersects the zones of oblique separations of the boundary layer induced by the side-wedge shock waves prior to a place of interaction of the latter with the ramp-wedge shock wave at the plane of symmetry. The pressure distribution on this wedge, both on the right and left from the plane of symmetry, demonstrates plateaus typical of the laminar separation. On the side wedges the behavior of the separation lines and the pressure distribution in the measurement cross section experience the influence of tip effects. (The separation lines curve upstream at the side edges; see Fig. 5.) Nevertheless, a plateau is again observed in the pressure distribution (Fig. 7c). The

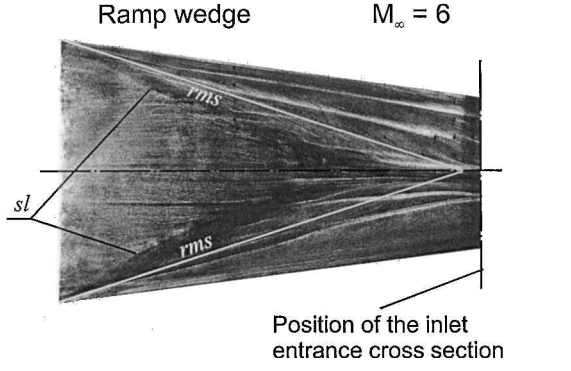

Fig. 6 Oil-film picture of limiting streamlines on the ramp wedge surface: $M_\infty = 6$ and no boundary-layer tripping.

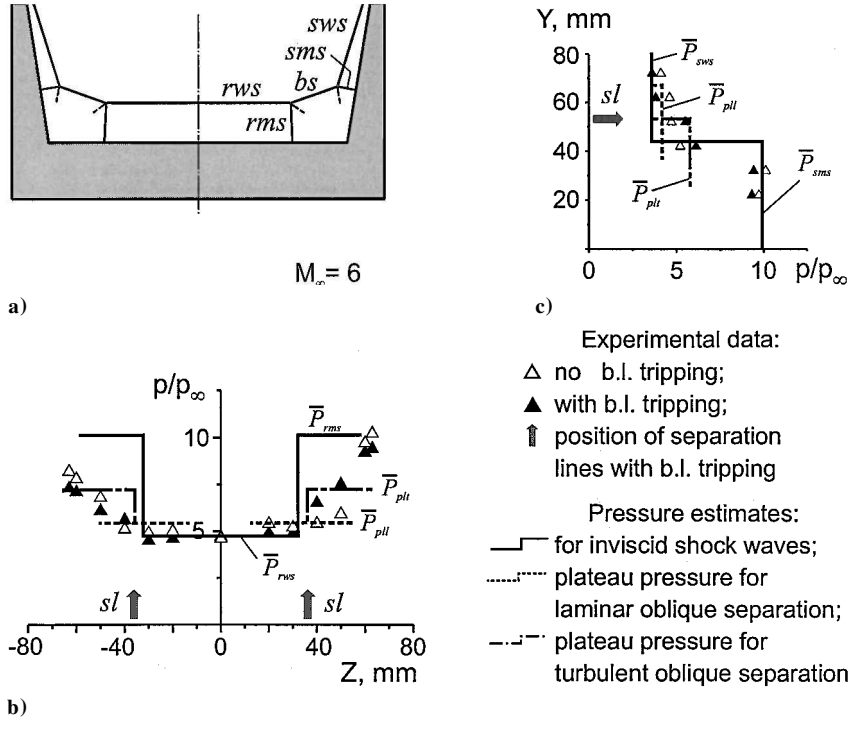

Fig. 7 Pressure distribution in the measurement cross section $x = 105$ mm for $M_\infty = 6$ in T-313.

plateau pressure level in all cases is in good agreement with the calculated estimate $\bar{p}_{pII}$ (4) for an oblique laminar separation.

2. Tests with Boundary-Layer Tripping

Boundary-layer tripping at high supersonic velocities is somewhat difficult. In particular, widely used sandpaper trips had failed for $M_\infty = 6$ in the T-313 wind tunnel. Therefore, grate-type trips[28] were tried out for the model considered at $M_\infty = 6$ in T-313. Their effectiveness was quite satisfactory, and they were also used in tests in IT-302M. The trips were made in the form of stainless sheet strips 0.15 mm thick with three rows of jag holes of different diameter d_j made by a punch. On the ramp wedge the trip width was 10 mm, and its leading edge was located at a distance of 10 mm from the leading edge of the wedge; the corresponding dimensions of trips on the side swept compression wedges were 7 and 7.2 mm, respectively. Diameters of the jag holes were chosen such that the jag height was $h_j \approx 0.5$ mm near the leading edge and $h_j \approx 1.0$ mm in the middle and near the trailing edge of the trip. This means that the trips had a cross wedge-shaped profile suitable to place them behind shock waves formed at the leading edges of the compression wedges. The spanwise step of holes was about $4 \cdot (d_j)_{max}$, and the holes were staggered in the streamwise direction. When the model was tested in T-313, the trips were glued and were additionally fixed by miniature rivets; in IT-302M they were fixed by point welding.

The efficiency of boundary-layer trips for $M_\infty = 6$ is demonstrated in Fig. 8, which shows, in comparison, oblique separation lines obtained in tests of the model in both wind tunnels with and without boundary-layer tripping. The separation lines are drawn, for simplicity, schematically but in a scale, based on the oil-film pictures obtained. The views on the ramp and side wedges along the directions normal to the compression planes are shown. The same figure shows the calculated position of the glancing shock wave *rms* and *sms* responsible for separation and the line of oblique separation for a turbulent boundary layer calculated by formula (2). The separation lines obtained with boundary-layer tripping are almost rectilinear, and their slope coincides with the calculated estimates. These properties of the separation lines characterize the boundary layer as fully developed turbulent. The latter is also confirmed by the pressure distribution in the measurement cross section $x = 105$ mm

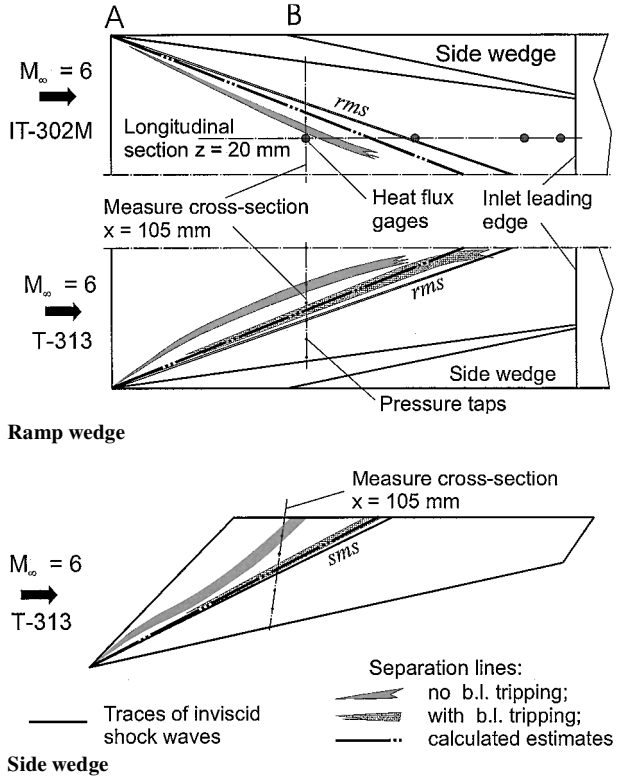

Fig. 8 Configuration of separation lines on the ramp wedge for $M_\infty = 6$ in IT-302M and T-313.

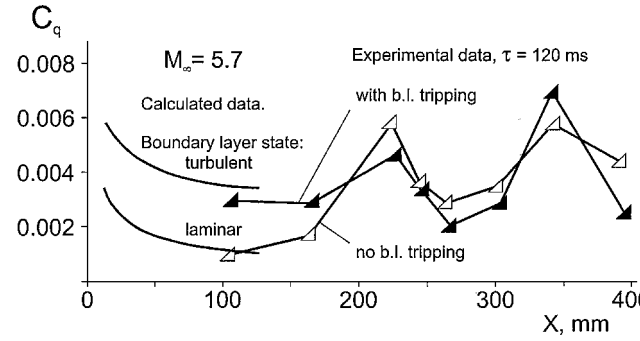

Fig. 9 Lengthwise distribution of heat fluxes in the longitudinal section z = 20 mm for M_∞ = 5.7 in IT-302M.

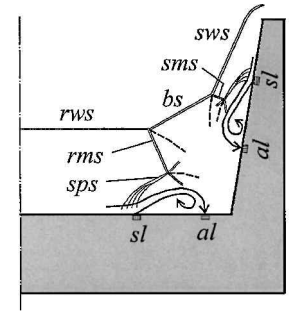

Fig. 10 Reconstructed crossflow structure.

for $M_\infty = 6$, which is shown in Fig. 7, where the test results without and with boundary-layer tripping are compared. For the latter case the arrows indicate the cross-sectional position of the separation lines *sl* determined by the oil-film spectra. The experimental level of pressure on the ramp wedge immediately behind these lines is in good agreement with the calculated estimate $\bar{p}_{plt}$ [Eq. (1)] for an oblique turbulent separation.

The efficiency of boundary-layer trips in tests in the hotshot wind tunnel IT-302M can also be evaluated by the results of heat-flux measurement at $M_\infty = 5.7$. Figure 9 shows the distribution of the heat-flux coefficient c_q on the ramp compression wedge and on the lower wall of the model duct in the longitudinal plane $z = 20$ mm. The data correspond to the measurement time interval of 110–120 ms at the end of wind-tunnel operation regime. Figure 9 also shows the calculated heat fluxes for the laminar and turbulent boundary layer on a smooth plate, which were obtained in accordance with Refs. 29 and 30. The plane $z = 20$ mm intersects the lines of oblique separation of the boundary layer, induced by the side shock wave *rms*, downstream of the measurement cross section $x = 105$ mm (Fig. 8), and the calculated values should be compared with experimental data at the first measurement point because only this point does not experience the effect of this oblique separation. Good agreement of the results can be noted. In particular, this indicates that a flow regime with a developed turbulent boundary layer forms at the external compression wedges of the inlet in the case of model testing with boundary-layer tripping in IT-302M. Similar results were also obtained for $M_\infty = 8$.

Thus, the tests conducted give grounds to believe that the grate-type trips ensure the flow around the external compression section of the model inlet with a turbulent boundary layer both at $M_\infty = 6$ in T-313 and at $M_\infty = 6$ and 8 in IT-302M.

3. Structure of Shock–Shock Interaction in Flow over the Inlet Wedges

The crossflow pattern over the compression wedges forming from the leading edges to the measurement cross section $x = 105$ mm and reconstructed according to the data obtained can be represented as shown in Fig. 10. Under actual conditions the structure of the interacting shock waves *rws* and *sws* forming in the inviscid flow is complicated by oblique separations of the boundary layer induced on the ramp and side compression wedges by the glancing shock waves *rms* and *sms*. These separations with helical vortices inside them form beginning from the dihedral corner vertices of the inlet;

on wedge surfaces they show themselves by swept lines of separation *sl* and attachment *al*. It can also be assumed that separation-induced shock waves *sps* form along the oblique separation lines *sl* in this case. The separation shock interacts with the reflected shock *rms* or *sms* with the forming, in a cross section, of a λ–shaped shock configuration including a rear shock, which is typical for a two-dimensional separation induced by the shock–boundary-layer interaction. The crossflow topology, determined in this instance by reconstruction, is analogous to that visualized in Ref. 31 with the use of planar laser scattering (PLS). A model used in that work for triple-shock experiments included a ramp ($\delta_{rw} = 10$ deg) and non-swept side ($\delta_{sw} = 15$ deg) compression wedges and was tested at $M_\infty = 3.85$, with the ramp wedge mounted on a flat plate. That is, there was a rather thick turbulent boundary layer in front of this ramp wedge in contrast to the inlet considered. In the crossflow image presented in Ref. 31, the interaction of the ramp and side shocks is observed, which results in the formation of a Mach shock configuration including a bridging shock *bs* and reflected shocks *rms* and *sms*, both the latter bifurcate into a separation and rear shocks with forming a λ–shaped shock configuration. Except for the similar topology, there are no other certain flowfield details that could be revealed from a comparison of the reconstructed crossflow pattern with the PLS image.

The transverse dimensions of separation regions on the ramp wedge and strength of the vorteciesincrease downstream. The glancing shock waves *rms*, *rms*′, the separation shock waves *sps*, *sps*′, and vortices inside the oblique separations are directed toward the plane of symmetry and impinge onto each other at the plane of symmetry and interact here, in a central glancing-shock/oblique-separation interaction region.

It is evident that the overall structure of flow over the inlet considered, which is characterized by occurrences of crossing glancing shock waves, is similar to that for an inlet with side compression wedges as inlets already mentioned.[5–9] Simulation of such flows, both experimental and numerical with the use of Navier–Stokes equations, has been considered in many papers. In analyzing this overall flow structure in the present investigation, the authors relied on Refs. 31–36. Note that most authors of the said references consider the flows over fins (vertical compression wedges) with rather large angles, in particular, $\delta_{sw} = 15$ deg, which are mounted on a flat plate with a developed turbulent boundary layer. That is why there are no specific data in these papers that could be compared directly with the data obtained.

One of the special features of flow over an inlet with side compression wedges investigated in the present paper is the laminar, laminar-turbulent, or artificially tripped boundary layer. As was already shown, the lines of oblique separations induced by glancing side shock waves *rms*, which emanate from the corner vertices, can be arc shaped, S shaped, or almost rectilinear depending on the state of the boundary layer on the ramp-wedge surface of the inlet considered. Regardless of their shape, they curve smoothly toward the plane of symmetry while they approach the latter. Corresponding to this behavior of the separation lines, the helical vortices forming in oblique separation regions deflect to a direction parallel to the plane of symmetry when approaching the latter and propagate far downstream. The oil-flow patterns obtained in tests with a natural predominantly turbulent ($M_\infty = 4$) or a fully turbulent (tripped, $M_\infty = 6$) boundary layer are close, in general topologically, to that shown, for instance, in Ref. 32 for side wedges with angles $\delta_{sw} = 11$ deg.

The limited transverse and longitudinal dimensions of the flow region with intersection of shock waves are important for the flow over the inlet considered as compared to configurations used in Refs. 31–36 for investigations of flows with crossing shock waves. First, tip and edge effects from the side compression wedges occur

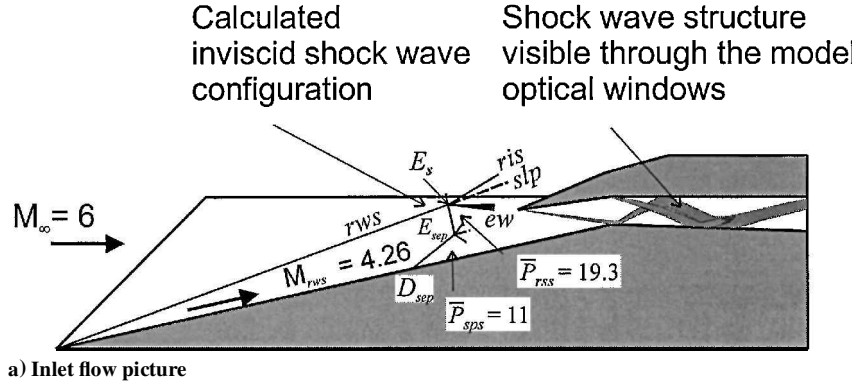

a) Inlet flow picture

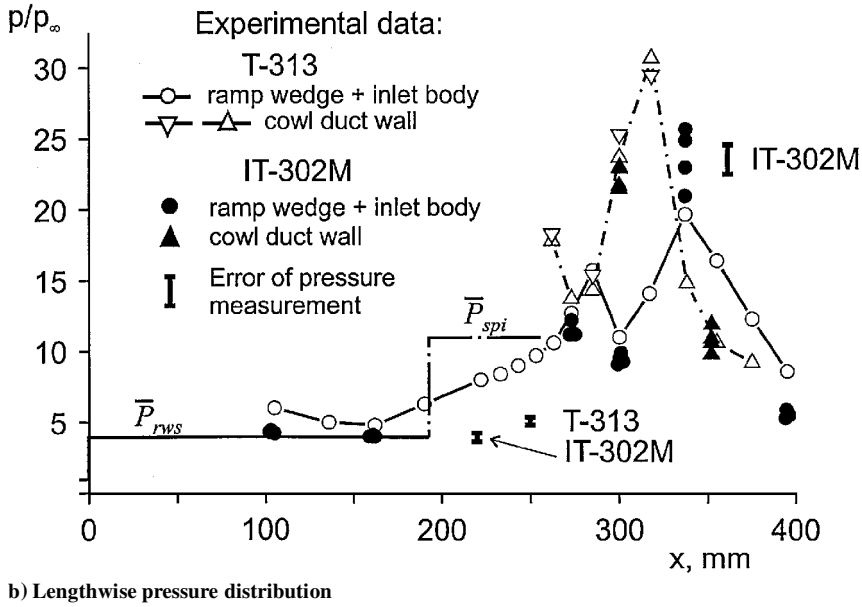

b) Lengthwise pressure distribution

Fig. 11 In the plane of symmetry for $M_\infty = 6$ in T-313 and IT-302M.

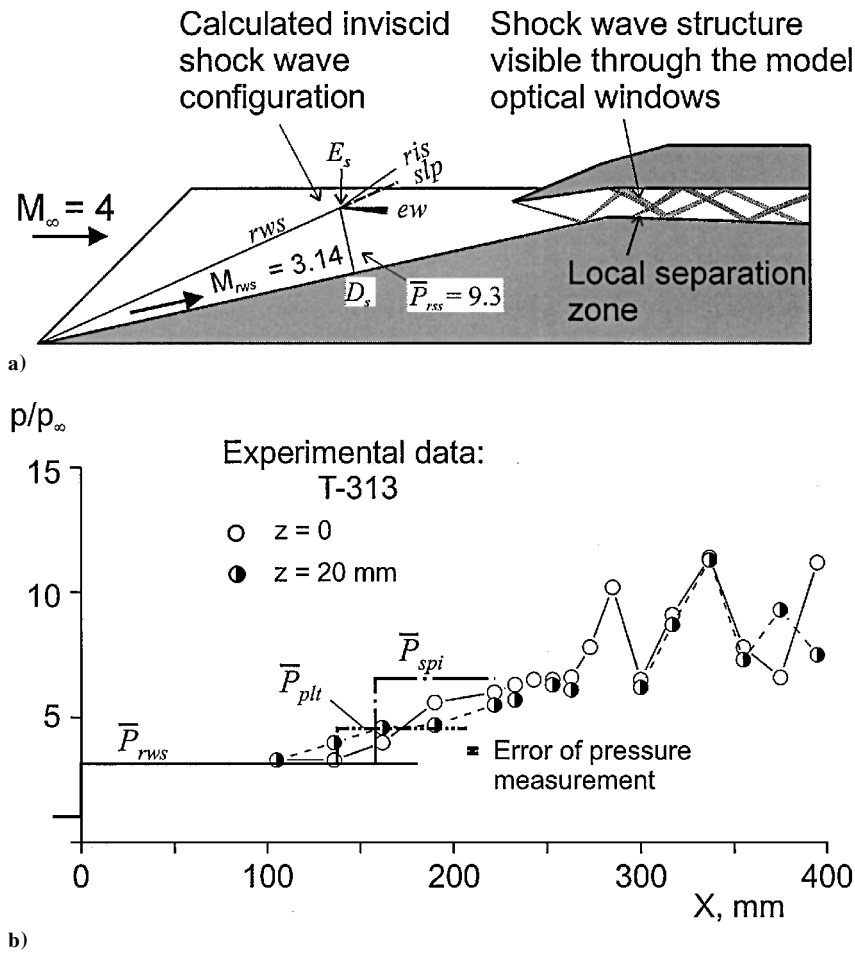

Fig. 12 In longitudinal sections z = 0 and 20 mm for M_∞ = 4 in T-313: a) inlet flow picture in the plane of symmetry and b) lengthwise pressure distribution.

in the central region of interaction of the glancing shock waves *rms* and oblique separations induced by them. Second, gasdynamic structures arising as a result of this interaction and developing downstream come, behind the inlet entrance, under the action of the shock wave from the cowl lip.

The actual flow pattern of interaction at the plane of symmetry of the side shock waves and quasi-conical structures of turbulent separation emanating from the vertices of the dihedral corners is very complicated. There is a set of works where such flow patterns were studied in detail, for $M_\infty = 3$, 3.85, and 4, experimentally[33] and experimentally and numerically, by solving the Navier–Stokes equations.[34–36] Unfortunately, the results of these papers cannot directly be used for analysis of the present experimental data.

The interaction of the glancing side shock waves *rms* with each other and with the boundary layer in the central region is evidently manifested in a lengthwise pressure distribution. And only such experimental distributions that were obtained in the presented work can be used for analysis of interaction of the crossing side shock waves and quasi-conical structures.

The pressure distribution in the plane of symmetry $z = 0$ is shown in Fig. 11 for $M_\infty = 6$ (tests of the model with boundary-layer tripping in T-313 and IT-302M) and in Fig. 12 for $M_\infty = 4$ (a test in T-313 with natural development of the boundary layer). In the latter case the pressure distribution in the longitudinal section $z = 20$ mm is also shown. In these figures the pressure distributions (Figs. 11b and 12b) are shown together with the model contour in the plane of symmetry and the calculated configuration of shock waves for inviscid flow over the compression wedges (Figs. 11a and 12a). In Figs. 11b and 12b one can see a gradual pressure increase in the region of intersection of the shock waves *rms* at the plane of symmetry, and the degree of this pressure increase behind the region of interaction is significantly lower than the calculated pressure behind the shock waves *rss* that arise as a result of reflection of shock waves *rms* at the line $E_s D_s$. The shock waves *rss* are shown in Fig. 3c; the levels $\bar{p}_{rss} \approx 19.3$ for $M_\infty = 6$ and $\bar{p}_{rss} \approx 9.3$ for $M_\infty = 4$ are marked in Figs. 11a and 12a.

Experimental pressure distributions in the longitudinal directions, particularly in the plane of symmetry, were compared with a possible change in the pressure level estimated for the central region of interaction in the case of the turbulent boundary layer with the use of the following simple assumptions. It was assumed that the separation shocks *sps* just mentioned form along rectilinear swept separation lines *sl* as spatially oriented plane shock waves with the pressure behind them equal to the plateau pressure. The position of the separation lines was estimated as just indicated, using formula (2). With the parameters of the separation shocks *sps* being known, one can calculate their intersection and reflection from the plane of symmetry. Thus, a possible stepwise increase in pressure and the characteristic dimensions of the zone of interaction of quasi-conical separations at the plane of symmetry was evaluated. The calculated structure of the interacting separation shock waves with the line $E_{sep} D_{sep}$ of their intersection at the plane of symmetry for $M_\infty = 6$ is shown in Fig. 11a, and the pressure level $\bar{p}_{spi} \approx 11$ after the interaction of the separation shock waves *sps* is marked in Fig. 11b. The experimental value of pressure in this region approaches this calculated estimate only at $x = 250$–260 mm.

As was just noted, S-shaped lines of oblique shock-induced separations forming in the case of the laminar-turbulent state of the boundary layer are typical of $M_\infty = 4$. The longitudinal section $z = 20$ mm intersects the zone of such an oblique separation prior to intersection of the shock waves *rms* in the plane of symmetry. In this longitudinal section, at $x = 160$–190 mm a pressure plateau typical of the oblique separation region is observed. The pressure level here is in good agreement with the calculated $\bar{p}_{plt}$ of the pressure plateau for an oblique turbulent separation by formula (1). The value $\bar{p}_{plt}$ is also marked in Fig. 12b for this longitudinal section.

The experimental level of pressure in the plane of symmetry in the region downstream of interaction of the shock waves *sps* and *rms* asymptotically approaches the calculated estimate $\bar{p}_{spi} \approx 6.5$ for $x = 240$–260 mm. This means that the conclusions drawn for $M_\infty = 6$ from a comparison of the experimental pressure increase and its calculated levels in the central interaction region are also reasonable for $M_\infty = 4$.

One more cause for the gradual pressure increase in the zone of central interaction, as compared to the stepwise increase in calculated estimates, can be assumed. It is that the separation shock waves form presumably as a result of focusing compression waves arising in the boundary layer along the separation lines, and, obviously, they are not planar. Hence, the pressure distribution in the plane of symmetry rather corresponds to interaction of fairly extended compression waves. Another possible cause is that the inviscid reflected shock waves *rms* in a real flow are not planar either but are transversely curved, and their interaction at the plane of symmetry along the nonstraight line $E_s D_s$ results in emergence of disturbances in the form of compression waves.

C. Flow Structure at the Entrance and in the Duct

It follows from the analysis of the shock structure for the inviscid flow that flowfield nonuniformity at the duct entrance is caused first by multiple interacting shocks in front of the inlet entrance. In particular, the shock waves *rss* reflected from the plane of symmetry and "cutting" the leading edge of the cowl lip should be noted, as is shown in Fig. 3c. It is evident from the experimental data just discussed that viscous features significantly complicate this flowfield nonuniformity at the duct entrance. This is caused by the fact that the glancing shock waves induce oblique separations of the boundary layer with forming of powerful streamwise helical vortices in them, and a complex interaction of these structures at the plane of symmetry occurs.

The flow patterns in the model duct in the plane of symmetry, which was obtained from the schlieren pictures, are schematically shown in Fig. 11a for $M_\infty = 6$ and in Fig. 12a for $M_\infty = 4$. A system of X-shaped shock waves forms in the duct, including those shocks that arise on the leading edge of the cowl lip and on the bend of the cowl wall, subsequent reflections of shocks from the walls, and their interaction with each other. Note that the shock waves forming on the rectilinear leading edge and the rib of the cowl bend are not planar because of the flow nonuniformity at the entrance. In addition, the reflected shock waves are "smeared" in a real flow because their reflection from the walls occurs through the boundary layer; actually, X-shaped compression waves are observed, as is shown in Figs. 4, 11a, and 12a. A comparison of the wave structure of the internal flow and the pressure distribution in the plane of symmetry behind the entrance cross section in Figs. 11 and 12 offers an explanation to the pressure peaks corresponding to the places where shock waves come on the duct walls.

Concerning the flow pattern at the entrance and in the inlet duct, we can note the following on the basis of oil-film visualization. Downstream of the entrance cross section, the internal shock wave emanating from the rectilinear leading edge of the cowl lip interacts with the shock waves *rss* arriving here; as a result, obviously, a system of spatially oriented and intersecting shock waves forms. At the places where these shock waves come on the ramp surface, a complex spanwise extended separation of the boundary layer, with a waved separation line, occurs, as is exemplified by Fig. 5. It includes the zones of three-dimensional (oblique) separations induced by the glancing shock waves *rss* and the zones of two-dimensional (nonoblique or transverse) separation induced by the shock wave from the cowl lip. The emergence of a shock wave on the lower wall in the throat behind the angle of expansion should be noted, as is seen from the shock-wave structure in the duct, which is shown in Fig. 4 for $M_\infty = 4$. Its appearance can be explained by the presence of a local transverse separation of the boundary layer induced by the shock wave coming from the line of the cowl wall bend in the throat, which is evidenced by the oil-film picture (Fig. 5). The internal shock waves arising on the leading edge and the contour bend of the cowl are glancing with respect to the side walls of the duct, and they induce oblique separations of the boundary layer on these walls. Oil-film visualization showed that helical vortices arising in these separation regions are directed first to the lower wall of the duct and then deflect and propagate downstream along the lower corner of the rectangular-cross-section duct.

The presence of the secondary reflected side shock waves *rss* and streamwise helical vortices at the inlet-duct entrance and the formation of X-shaped compression waves and vortices of such a kind along the side walls in the duct lead, obviously, to a significant nonuniformity of the flowfield inside the duct and at the inlet exit. The latter is confirmed by the distribution of the pressure p_0' measured over the exit cross section by a rake with 25 pitot tubes over half of the exit cross section. The data obtained in T-313 for $M_\infty = 4$ and 6 are plotted in Fig. 13, where the pitot pressure p_0' is normalized to the freestream total pressure $p_{0\infty}$. At $M_\infty = 4$ a convex character of the pressure profile with low values of p_0' near the lower and upper walls is observed in the central part of the cross section, which

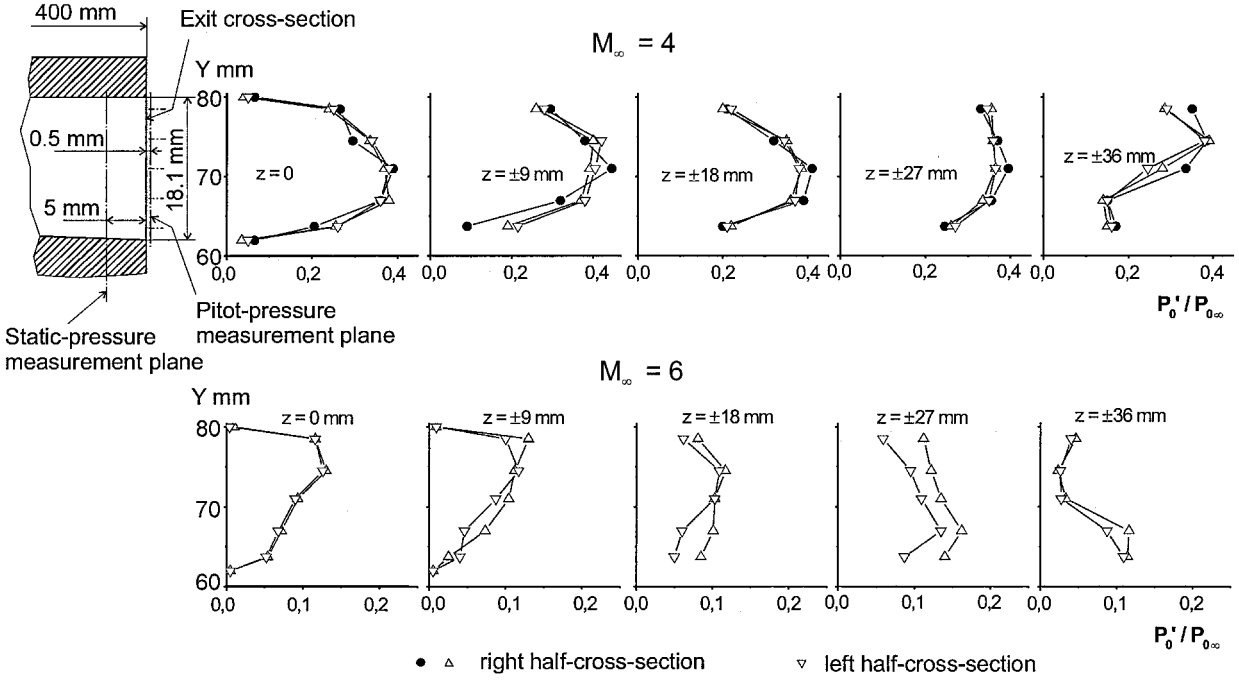

Fig. 13 Pitot-pressure distribution over the inlet exit cross section for $M_\infty = 4$ and 6 in T-313.

can be attributed to two factors. First, the pitot tubes located near the walls measure the stagnation pressure in the boundary layer; second, ahead of the survey cross section there are compression waves near the upper and lower walls of the duct, which were observed by optical visualization of the duct flow (Fig. 5). For $M_\infty = 6$ the same factors affect the shape of the pressure profiles in the central part of the cross section, but the maximum of p'_0 is shifted toward the upper wall correspondingly to the movement of the compression wave (see Fig. 11a). S-shaped pressure profiles p'_0 are observed near the side walls ($z = \pm 36$ mm) for both Mach numbers $M_\infty = 4$ and 6. The deformation of these profiles as compared to the central part of the cross section is related to the vortices just mentioned arising as a result of the oblique shock-induced separation of the boundary layer on the side walls.

D. Some Special Features of the Inlet Flow at $M_\infty = 6$ in IT-302M

The special features of the external flow around compression wedges and internal duct flow just described, which were revealed by inlet testing in T-313, explain to a large extent the measurement results obtained in IT-302M.

The lengthwise distributions of heat fluxes c_q in the longitudinal section $z = 20$ mm, which was measured in IT-302M at $M_\infty = 6$ in model testing without and with boundary-layer tripping on the ramp wedge, were shown in Fig. 9. They were already discussed in connection with the analysis of the heat-flux level at the first measurement point that was not affected by oblique separation, which demonstrated the efficiency of boundary-layer trips. Farther downstream, a wavy character of the heat-flux distribution with two maxima is observed. The first maximum is related to the line of boundary-layer reattachment in the zone of oblique separation induced by the side shock wave *rms*. The second maximum is located in the duct, at the place where the shock wave from the cowl bend hits on the lower wall (Fig. 11a). The difference in the levels of heat-flux minima and maxima obtained in tests without and with boundary-layer tripping is about 30%, that is, in these cases the viscous near-wall flow has a different character at the entrance and in the inlet duct as it occurs at the external compression wedges.

A comparison of the lengthwise pressure distribution in the plane of symmetry $z = 0$ for $M_\infty = 6$ in tests conducted in T-313 and IT-302M is shown in Fig. 11b. The pressures measured in IT-302M are averaged over the time interval $\tau \sim 80$–110 ms, which corresponds to a quasi-steady regime of wind-tunnel operation with almost constant freestream parameters. As was discussed for T-313 data, there are maxima in the pressure distribution along the duct at the places where shock waves come on duct walls and minima between them. Note that the pressure measurement taps for both the models tested in T-313 and particularly in IT-302M were too sparsely placed, and this did not allow a more accurate localization of the pressure extrema; nevertheless, their positions in both wind tunnels roughly correlate. A greater difference in pressure is observed immediately behind the inlet throat (where the shock wave from the cowl lip hits on the lower wall) and near the exit cross section of the inlet. This is apparently related to some difference in flow parameters in T-313 and IT-302M, mainly, Reynolds numbers. In T-313 experiments the Mach and Reynolds numbers were $M_\infty = 5.85$–6.0 and $Re_{1\infty} = (1.8\text{–}2) \times 10^7$ 1/m; the corresponding values in IT-302M were $M_\infty = 5.6$–5.8 and $Re_{1\infty} = (2\text{–}2.5) \times 10^6$ 1/m. This was responsible for somewhat different evolution of separation regions, their length, the flow downstream of them, and hence, different levels of pressure measured at an identical x coordinate along the model.

VI. Conclusions

The flow around a three-dimensional inlet with a ramp wedge and side compression wedges has been studied experimentally in two wind tunnels of different operation within the Mach range $M_\infty = 4$–8. The structure of the flow around the external compression wedges and in the inlet duct with a complex system of multiple shock waves three-dimensionally interacting with each other and with the boundary layer has been revealed. A characteristic feature, in particular, is the presence of glancing shock waves, which induce oblique separations of the boundary layer, where intense helical vortices propagating far downstream form. A complex system of multiple shock waves, expansion waves, and vortex structures leads to significant nonuniformity of the flowfield at the inlet-duct entrance and exit.

Analytical calculations of the inviscid flow structure in the initial compression region of the airstream captured by the inlet have been carried out including semi-empirical correlation for parameters of oblique separations of the boundary layer. Estimated possible shock-wave positions, pressure levels, and heat fluxes in the flow over the compression wedges including the zones of oblique separation of the boundary layer are in good agreement with experimental data. The calculations were helpful for understanding of the formation, as a whole, of the flow structure around the inlet.

The results of oil-film visualization of the surface streamlines and the measurement of pressures and heat fluxes on the model surface have confirmed the efficiency of the method of boundary-layer tripping used. Model tests with boundary-layer tripping at $M_\infty = 6$ in T-313 and at $M_\infty = 6$ and 8 in IT-302M have shown that flow regimes forming in this case correspond to a rather developed turbulent state of the boundary layer on the external compression wedges.

Model tests with boundary-layer tripping for a Mach number $M_\infty = 6$ in both wind tunnels ensured a qualitatively identical flow regime over the inlet, which allowed a direct comparison of the surface-pressure distributions and other flow characteristics obtained in wind tunnels with different operation principles. As a whole, experimental data in both wind tunnels are in good qualitative agreement by taking into account some quantitative difference mainly attributed to the difference in unit Reynolds numbers.

Acknowledgments

This work was sponsored by the French Ministry of Defense and Dassault Aviation under Contract 42F04813.

References

[1]Chalot, F., Rostand, P., Perrier, P., Goonko, Y., Kharitonov, A., Latypov, A., Mazhul, I., and Yaroslavtsev, M., "Validation of Global Aeropropulsive Characteristics of Integrated Configurations," AIAA Paper 98-1624, April 1998.

[2]Adamov, N., Goonko, Y., Kharitonov, A., Latypov, A., Mazhul, I., Yaroslavtsev, M., Chalot, F., Rostand, P., and Perrier, P., "Study on Drag-Thrust Forces of a Scramjet Model in Blow-Down and Hot-Shot Wind Tunnels," *Proceedings of the International Conference on the Methods of Aerophysical Research (ICMAR'98)*, Inst. of Theoretical and Applied Mechanics, Novosibirsk, Russia, 1998, Pt. 3, pp. 3–9.

[3]Perrier, P., Rostand, P., and Stoufflet, B., "Integration of an Air-Breathing Hypersonic Airplane," AIAA Paper 93-5032, 1993.

[4]Perrier, P., and Rostand, P., "Hypersonic Air-Breathing Airplane Integration," AIAA Paper 94-3090, 1994.

[5]Hunt, J. L., Johnston, P. J., and Cubbage, J. M., "Hypersonic Air-Breathing Missile Concepts Under Study at Langley," AIAA Paper 82-316, 1982.

[6]Trexler, C. A., "Performance of an Inlet for an Integrated Scramjet Concept," *Journal of Aircraft*, Vol. 11, No. 9, 1974, pp. 588–591.

[7]Trexler, C. A., "Inlet Performance of the Integrated Langley Scramjet Module (Mach 2.3 to 7.6)," AIAA Paper 75-1212, 1975.

[8]Henry, J. R., and Anderson, G. Y., "Design Consideration for the Airframe-Integrated Scramjet," *Proceedings of the First International Symposium on Air-Breathing Engines*, 1972; *Review on Inlets of Airbreathing Engines for Hypersonic Flight Speeds*, Reviews-Translations-Annotations, No. 522, TsAGI, Moscow, 1977 (in Russian).

[9]Vinogradov, V. A., Stepanov, V. A., and Alexandrovich, E. V., "Numerical and Experimental Investigation of an Airframe-Integrated Inlet for High Velocities," AIAA Paper 89-2679, 1989.

[10]Dem'yanenko, V. S., Grigor'ev, V. D., Kharitonov, A. M., Pisarenko, K. I., and Volonikhin, I. I., "Supersonic Wind Tunnel T-313," *Aerophysical Studies*, Inst. of Theoretical and Applied Mechanics, Novosibirsk, Russia, 1972, pp. 8–11 (in Russian).

[11]Amelina, M. A., Brodetsky, M. D., Kharitonov, A. M., Ol'khovikov, G. P., Volonikhin, I. I., Vyshenkov, Y. I., and Zuenko, V. S., "Multichannel Pressure Meter MID-100," *Techniques and Instrumentation for Aerodynamic Experiment*, Inst. of Theoretical and Applied Mechanics, Novosibirsk, Russia, 1978, pp. 98–113 (in Russian).

[12]Brodetsky, M. D., Brouk, S. M., and Makhnin, A. M., "Study on Measurement Errors of Reduced Pressure Coefficients at Supersonic Velocities," *Aerodynamic Studies of Non-Plane Wings*, Inst. of Theoretical and Applied Mechanics, Novosibirsk, Russia, 1977, pp. 94–113 (in Russian).

[13]Puzyrev, L. N., and Yaroslavtsev, M. I., "Stabilization of Gas Parameters in Plenum Chamber of Hot-Shot Wind Tunnel," *Izvestiya SB AS USSR, Seriya Technicheskikh Nauk*, Issue 5, 1990, pp. 135–140 (in Russian).

[14]Petunin, A. N., *Techniques and Instrumentation for Measurement of Gas Flows*, Mashinostroenie, Moscow, 1972, pp. 158–208 (in Russian).

[15]Ledford, R. L., "A Gauge for Measurement of Heat Flux in Hypersonic Wind Tunnels," *Advances in Hypervelocity Techniques*, *Proceedings of the Second Symposium on Hypervelocity Techniques*, edited by A. M. Krill, Plenum, New York, 1962; Mashinostroenie, Moscow, 1965, pp. 458–449 (in Russian).

[16]Bogdanov, V. V., and Pleshakova, L. A., "Errors of Heat Flux Reconstruction by Calorimetric Convertors," *Trudy TsAGI*, No. 1847, 1977, pp. 21–33 (in Russian).

[17]Goonko, Y., Kharitonov, A., Latypov, A., Mazhul, I., and Yaroslavtsev, M., "A Technique for Determination of Heat Fluxes and Force Characteristics of Ramjet/Scramjet Models in a Hot-Shot Wind Tunnel," *Proceedings of the International Conference on the Methods of Aerophysical Research (ICMAR'2000),* Siberian Branch, Russian Academy of Sciences, Novosibirsk, Russia, 2000, Pt. 3, pp. 51–58.

[18]Goonko, Y. P., and Markelov, G. N., "Application of Relations for an Oblique Shock Wave in the Two-Dimensional Flow to Problems on Plane Shock Waves of General Spatial Orientation," Inst. of Theoretical and Applied Mechanics, Preprint 15-89, Novosibirsk, Russia, 1989 (in Russian).

[19]Goonko, Y. P., Markelov, G. N., and Shashkin, A. P., "Gas-Dynamic Design of Waveriders with Convergent Compression Surfaces and Inlets," *Siberian Physical-Technical Journal*, No. 4, 1993, pp. 47–55 (in Russian).

[20]Kornilov, V. I., Levchenko, V. I., and Kharitonov, A. M., "An Investigation of Boundary Layer Transition on a Wing Airfoil at Supersonic Velocities," *Izvestiya SB AS USSR, Seriya Technicheskikh Nauk*, No. 3, Issue 1, 1971, pp. 15–20 (in Russian).

[21]Kalinina, S. V., and Kornilov, V. I., "Effects of Sweep Angle and Unit Reynolds Number on Transition of Boundary Layer at Supersonic Speeds," *Prikladnaya Mekhanika i Tekhnicheskaya Physika*, No. 1, 1973, pp. 159–162 (in Russian).

[22]Struminsky, V. V., Kharitonov, A. M., and Chernykh, V. V., "Experimental Study on Transition of Laminar Boundary Layer to Turbulent One at Supersonic Velocities," *Mechanika Zhidkosti i Gasa*, No. 2, 1972, pp. 30–34 (in Russian).

[23]Dem'yanenko, V. S., "Experimental Study of Three-Dimensional Supersonic Flows in Region of Interferaction Between Intersecting Plane Surfaces," Ph.D. Dissertation, Inst. of Theoretical and Applied Mechanics, Novosibirsk, Russia, 1973 (in Russian).

[24]Dem'yanenko, V. S., and Igoumnov, V. A., "Three-Dimensional Interaction of Shock Waves with Turbulent Bounadary Layer in Corner Flows," *Izvestiya SB AS USSR, Seriya Technicheskikh Nauk*, No. 8, Issue 2, 1975, pp. 56–62 (in Russian).

[25]Korkegi, R. H., "Comparison of Shock-Induced Two- and Three-Dimensional Incipient Turbulent Separation," *AIAA Journal*, Vol. 13, No. 4, 1975, pp. 534–535.

[26]Degrez, G., and Ginoux, J. J., "Surface Phenomena in Three-Dimensional Wave Laminar Boundary-Layer Interaction," *AIAA Journal*, Vol. 22, No. 12, 1984, pp. 1764–1769.

[27]Belyanin, N. M., "Theory of Boundary Layer," *Applied Gas Dynamics*, edited by G. N. Abramovitch, Nauka, Moscow, 1976, pp. 276–360 (in Russian).

[28]Davlet-Kil'deev, R. Z., "Study on Transition of Boundary Layer on a Cone in Hypersonic Flow at Various Angles of Attack," *Trudy TsAGI*, No. 1881, 1977 (in Russian).

[29]Bashkin, V. A., "Calculation of Skin Friction and Heat Transfer Coefficients for Laminar Boundary Layer on Flat Plate, Cone, and Near Stagnation Point of Blunted Bodies Without Dissociation," *Trudy TsAGI*, No. 973, 1965 (in Russian).

[30]Kovalenko, V. M., "Calculation of Friction and Heat Transfer Coefficients for a Flat Plate in the Presence of Heat Transfer at Supersonic Speeds," *Trudy TsAGI*, No. 1084, 1967 (in Russian).

[31]Garrison, T. J., Settles, G. S., and Horstman, C. C., "Measurements of the Triple Shock Wave/Turbulent Boundary-Layer Interaction," *AIAA Journal*, Vol. 34, No. 1, 1996, pp. 57–64.

[32]Narayanswami, N., Knight, D. D., Bogdonoff, S. M., and Horstman, C. C., "Interactions Between Crossing Oblique Shocks and a Turbulent Boundary Layer," *AIAA Journal*, Vol. 30, No. 8, 1992, pp. 1945–1952.

[33]Kussoy, M. I., Horstman, K. C., and Horstman, C. C., "Hypersonic Crossing Shock-Wave/Turbulent-Boundary-Layer Interactions," *AIAA Journal*, Vol. 31, No. 12, 1993, pp. 2197–2203.

[34]Garrison, T. J., Settles, G. S., Narayanswami, N., and Knight, D. D., "Structure of Crossing Shock-Wave/Turbulent Boundary-Layer Interactions," *AIAA Journal*, Vol. 31, No. 12, 1993, pp. 2204–2211.

[35]Gaitonde, D., and Shang, J. S., "Structure of a Turbulent Double-Fin Interaction at Mach 4," *AIAA Journal*, Vol. 33, No. 12, 1995, pp. 2250–2258.

[36]Garrison, T. J., Settles, G. S., Narayanswami, N., Knight, D. D., and Horstman, C. C., "Flowfield Surveys and Computations of a Crossing Shock Wave/Boundary-Layer Interaction," *AIAA Journal*, Vol. 34, No. 1, 1996, pp. 50–56.

M. Sichel
Associate Editor